A Femtotesla Optical Magnetometer Suitable for Applications In Multi-channel Magnetic Imaging

Oleg Polyakov

Laser Teaching Center
November 2003

I. Introduction

Currently, many research fields such as medicine, biology, and geophysics, are in great demand for an inexpensive, small, and sensitive device that is capable of measuring tiny magnetic fields. The most modern system available that can measure such fields is the Superconductive Quantum Interference Device, or SQUID, which achieved a sensitivity of about 0.9-1.4 $fT/Hz^{1/2}$ [1, 2] . This value is know as the noise sensitivity and characterizes the magnetic field that can be measured with a signal to noise ratio equal to one in the bandwidth of 1 Hz. However, the most widely used low critical temperature (about 4.2 °K for liquid Helium), or low Tc, SQUID systems have many drawbacks; they require a $50,000- $100,000 large, non magnetic dewar, which is then cooled to a liquid helium temperature, making it bulky and hazardous and thus posing a problem both in its maintenance and price [3].

A relatively new method of measuring magnetic fields is with an optical magnetometer. First developed in the 1970's [4], they lagged in sensitivity compared to the SQUIDs, achieving a maximum of 1.8 $fT/Hz^{1/2}$ [5]. With the development of the Nonlinear Magneto-Optic Rotation method the estimated sensitivity was improved to about 0.3 $fT/Hz^{1/2}$ for a 500 cm^3 cell [6].

These types of magnetometers usually require an RF field applied through the alkali cell [8, 9] or use a very large-volume cell [10]. They have very high sensitivities but in addition have many drawbacks. The RF coil magnetometer can only be used to make single channel readings because in multi channel application, the mutual interference of multiple RF coils will disturb the readings, making this magnetometer inapplicable for the measurements of weak magnetic fields. The large cell magnetometer is impracticable for measurements with high spatial resolution and is typically used only in large-scale measurements in geophysics.

The major obstacle for even greater sensitivity was the spin relaxation of the atoms, which is when the atom loses its spin orientation due to collisions with other atoms. Recently a Spin Exchange Relaxation Free (SERF) magnetometer was developed, which has almost no spin exchange relaxation [7]. This magnetometer was based on a potassium vapor cell, which was selected for its special property of having the lowest spin relaxation between its molecules [7]. When working in an extremely small magnetic field environment, created by setting up multiple layers of magnetic shields, it was noted that due to the absence of spin exchange the relaxation time of the atoms was about 10^4 times greater than in non-SERF devices, providing a theoretical sensitivity of better than 0.01 $fT/Hz^{1/2}$. The actual measured sensitivity was a world record of 0.54 $fT/Hz^{1/2}$ achieved with a very compact magneto sensitive cell with the active volume of few cubic centimeters only. Unfortunately, the operation of such a magnetometer would require the use of expensive and heavy magnetic shields and the heating of the potassium cell to a high temperature, making the magnetometer unfit for practical applications in biology and medicine.

The goal of this project is to construct a SERF optical magnetometer based on a cesium cell, rather than a potassium cell as in the previous SERF magnetometer. Cesium was selected because it requires heating to a lower temperature than potassium to achieve the same sensitivity and would be more suitable for practical applications. In addition, the sensitivity dependence on temperature, pressure, and external magnetic field for the cesium SERF magnetometer was predicted theoretically but never tested experimentally. If these parameters were optimized to achieve not an absolute record but some moderate sensitivity in the presence of magnetic fields, it would then be possible to remove the magnetic shield. The removal of shields would allow the creation of inexpensive devices such as an array of optical magnetometers that could be used in applications for cardio and brain magnetic imaging.

II. Principles of all-optical magnetometer.

The operation of the magnetometer (see Fig.1) is based completely on the well known effect of mutual interaction between circularly polarized light and spin polarized atoms [7].

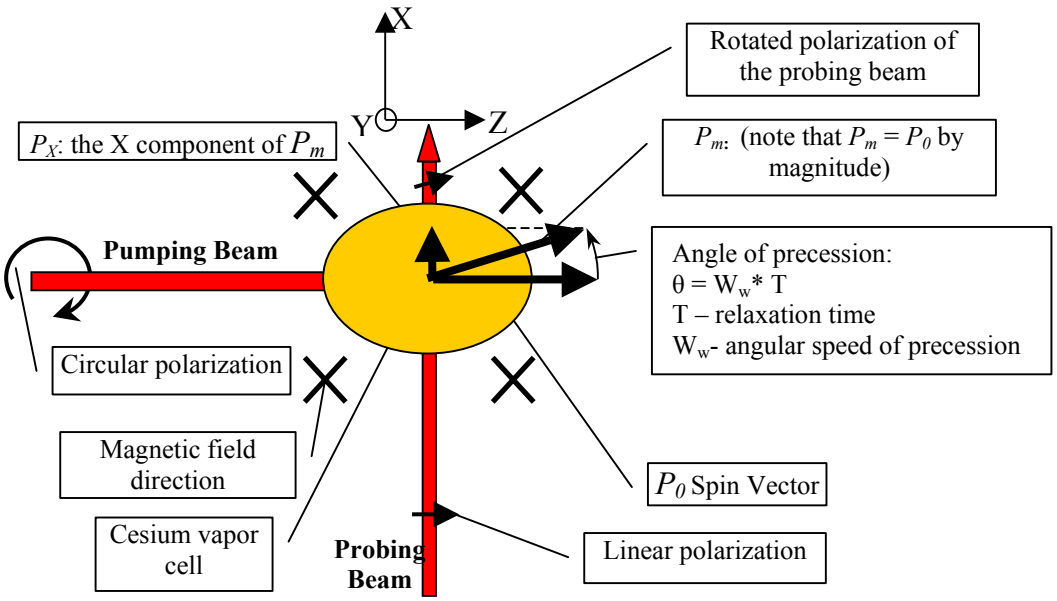

Fig 1. Operation principle of the optical magnetometer. The magnetic field is perpendicular to both the probing and the pumping beams. P_0 - initial polarization of the cesium atoms. P_m – precessing polarization spin. P_X – X-component of the spin that causes the rotation of the probing beam polarization.

When a powerful circularly polarized laser light, tuned to the main optical transition frequency between the $6S_{1/2}$ and $6P_{1/2}$ levels of the cesium D1 line, is incident upon a cesium atom, the atomic spin of the pumped up electrons becomes oriented in the direction of the propagating beam. This effect is called optical pumping.

If the pumping light illuminates the cesium cell in the Z-direction, then the spins of all the cesium atoms would eventually point in the Z-direction of the propagating beam and are said to be spin polarized with their spin polarization vector designated by P_0 (see Fig. 1).

An external magnetic field applied perpendicular to the pumping beam in the Y-direction would cause the polarization vector P_0 to precess around the direction of the magnetic field with Larmor frequency:

$$\omega_L = \gamma \bullet B \qquad (1)$$

Where γ=35.087 MHz/T is the cesium atom gyromagnetic ratio and B is the applied magnetic field to be measured. The spin vector P_0 will keep rotating with a constant angular velocity ω_L around the Y-axis until the atom collides with the wall or another atom and set the spin vector to an arbitrary orientation. The lifetime of the spin orientation can be characterized by the average effective relaxation time T_r that atoms spend in the spin-oriented state. During this time the spin would rotate by the angle

$$\alpha = \omega_L \bullet T_r \qquad (2)$$

And will take a new position P_m that has an X-direction component P_x orthogonal to the pumping beam and the magnetic field.

$$P_x = P_m \bullet Sin\ (\alpha) \qquad (3)$$

It should be noted that the total precession angle is always much less then one complete revolution due to the low value of either T_r or B and the spin never actually revolves around the magnetic field direction but just turns by the small angle so that $Sin(\alpha) \approx \alpha$. In this case P_x changes proportionally to the measured magnetic field B with the coefficient T_r that should be maximized to achieve better sensitivity.

Since P_x creates cesium vapor dichroism in the X-direction its value can then be measured by using a probing laser beam detuned from the main D1 absorption line to avoid pumping of atoms and rearranging them in the X-direction [11]. One of the ways to measure P_x is based on circular dichroism in X-direction.

A linearly polarized beam vector could be thought of as the superposition of 2 vectors going in circles: one spinning to the left and the other is spinning to the right. If one is to add these two rotating vectors one gets a vector going up and down with respect to time, which is equivalent to a propagating linearly polarized light beam.

If this linearly polarized light is incident upon the optically pumped spin polarized atoms with a precision created orthogonal component due to the magnetic field, the spinning component that is turning in the direction of the spin of the pumped atoms will experience a different index of refraction than the spinning component that is spinning opposite to the atomic spin. This slows down one component while speeding up the other one, creating a phase difference which in their superposition creates a turn in the overall linear polarization of the probing light. This turn of the polarization can be measured with an analyzer and a photo detector and this signal can be calibrated to indicate the strength of the applied magnetic field.

III. Experimental setup

The magnetometer (see Fig. 2) consists of the following modules:

A) Tunable laser source

One of the main tasks for the project was to build two independent laser sources for the pumping and the probing beams. These two laser modules were provided with controllable parameters such as temperature and injection current and were also adjustable in wavelength so it would be possible to tune the lasers to the D1 absorption line of the cesium atoms (see Fig.3). In addition collimation was provided for the beam since it diverges from the laser crystal at a 40° - 10° angle.

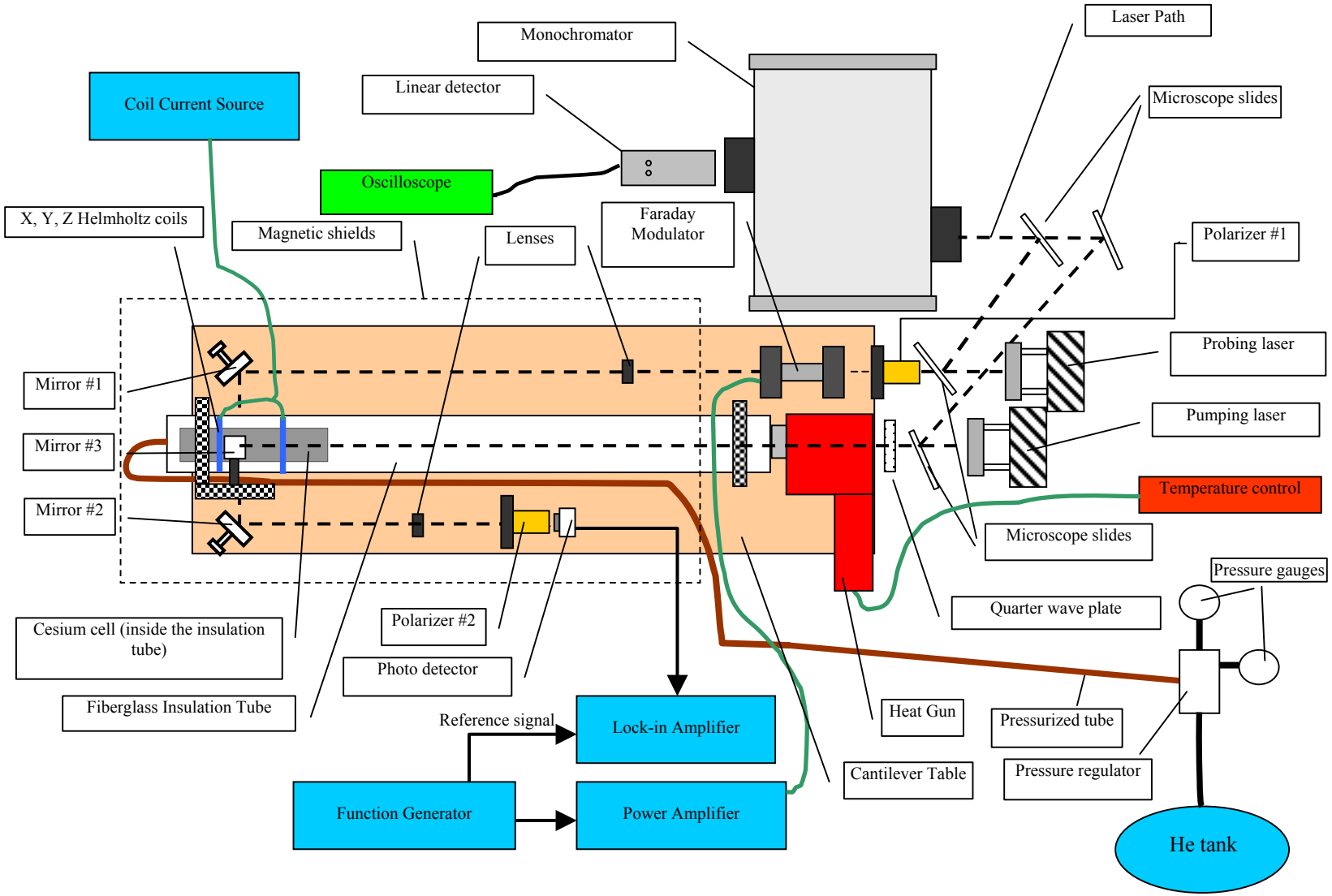

Fig 2. The block diagram of the magnetometer setup. The path of the laser beams is shown with dashed line. The left end of the cantilever table is located inside a double-wall magnetic shield.

The lasers that were used in this experiment were commercial diode lasers whose crystals were already installed onto a peltier element which facilitates the temperature control of the crystal. Two power supplies for the lasers were constructed which allowed setting of the injection current to the crystal and regulating the temperature by the PID (Proportional-Integral-Differential) controller.

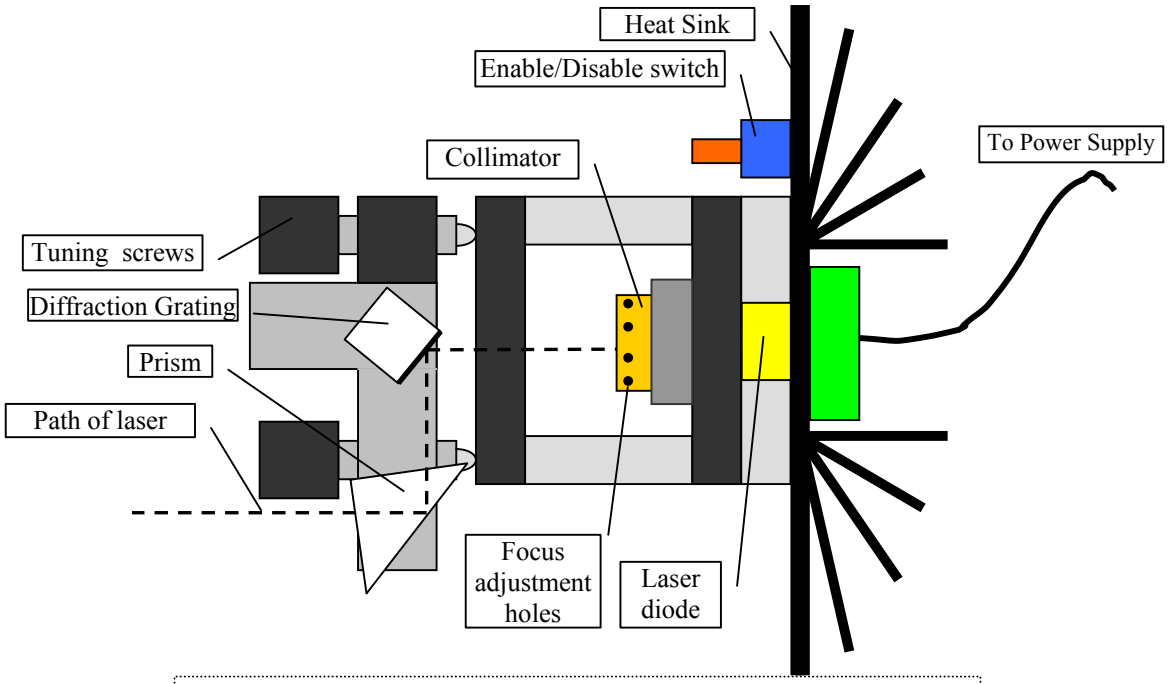

Fig 3. The configuration of the tunable diode laser module.

In order to collimate the beam a collimating lens was mounted on a fine threaded ring in front of the laser. The collimator was initially adjusted to form the sharpest possible spot at a distance of about 4 meters.

To form an external cavity for the laser radiation, we used a diffraction grating with 1600 rulings/mm installed in a Littrow configuration. In this configuration the grating sends its first order beam back into the laser crystal, thus providing a wavelength selective feedback [12, 13]. Since different wavelengths are dispersed by the grating at different angles, only those

wavelengths that reach the lasing cavity will be amplified. The light reflected by the grating into the zero order forms an output beam that leaves the external cavity as if it was reflected by a regular mirror. By using an adjusting screw it is possible to turn the diffraction grating along the spectrum of its first order very slowly and select the desired wavelength. We observed the spectrum of the laser radiation with the multi-channel linear detector installed at the output of the monochromator and connected to an oscilloscope. By the fine adjustment of the grating orientation and the collimating lens we were able to create such conditions that we observed only one bell-shaped line in the laser spectrum with a typical width of 0.2 nm.

Because, the resolution of our monochromator was about 0.2 nm, we could not see the 0.01 nm hyperfine laser mode structure of the mode separation for our external cavity. However, since the estimated absorption line width of the cesium is more then 0.03 nm, we can assume that at least several of the hyperfine laser modes will fall into the absorption line of the cesium and would provide the pumping of the cesium vapors.

Another helpful idea was to place the diffraction grating and a reflective surface (in our case a prism) onto the same platform, parallel to each other [13]. This guaranteed that when the platform is rotated, one could still select the desired wavelength, but not change the direction of the outgoing beam. This is extremely helpful because it eliminates a change of the beam direction when changing the wavelength.

B) The Cantilever Optical Table

The setup is located on an inch thick oak cantilever, which is mounted on a standard optical table and is horizontally suspended into two magnetic shields (see fig. 2). A major predicament for the construction of this cantilever was that no metallic parts could be present. It could be thought that such non magnetic metals as aluminum and brass could be used to secure

the components to the cantilever, but even those metals generate small magnetic fields from eddy currents inside them which can interfere with measurements. The solution for this problem was simple; plastic was used for the object holders and epoxy was used for the adhesive. Also the use of oak for the cantilever is a very good idea because it is extremely rigid along its fibers and also caries some properties of plastics like the ability to be drilled and threaded.

C) The cesium cell

The cesium vapor cell is a high pressure glass test tube with a Teflon plug connected to the open end. A 1/8" stainless steel tube is connected to the Teflon plug and provides the pressure to the cell. The cell was mounted on Teflon supports inside another 2" diameter glass tube connected to the insulation pipes leading to the hot air gun.

The temperature was regulated by the circulation of hot air produced by a hot air gun through fiberglass tubes around the cell and then releasing the used air into the laboratory. A thermocouple was attached to the cesium cell, giving a precise and rapid reading of the temperature. The temperature of the air was controlled manually with the variac, a transformer with regulated voltage, that modulated the voltage of the heating element in the hot gun. With this system we were able to set any temperature in the range 30˚C - 200 °C and maintain it with the accuracy ±2˚C.

The pressure inside the cell was created from a high pressure ultra high purity helium tank. A two-stage pressure regulator was attached between the helium tank and a pressure tube to manually set any pressure up to 3 atm. A flexible copper tube was used to connect the pressure regulator with the stainless steel tube which was connected to the cell. An additional valve was used for connecting the pressurization system to the vacuum pump which removed the air in the system before the ultra high purity helium was added

D) The laser light delivery system

The path of the pumping beam was as follows. It first passes through a microscope slide, which directs a portion of the beam into the monochromator for the spectrum monitoring. It then goes through a quarter wave plate the provides a circular polarization, then proceeds over and parallel to the insulation tubing, and is then reflected off mirror #2 downwards through an opening in the insulation tubing into the cesium cell.

The path of the probing beam is a little more complex than the pumping one. The path of the light is at the same height as the insulation tubing and is parallel to it. It first passes through a microscope slide, which reflects a small percentage into the monochromator. Then it passes through a polarizer #1, which is set up parallel to the laser's linear polarization, to a Faraday modulator, whose function will be described later. Afterwards the light is reflected off mirror #1 into the cesium cell, and then it is reflected off mirror #2 into a lens which focuses the beam though polarizer #2 onto the photo detector (see fig. 2).

E) Monochromator

The light is reflected into the monochromator (model 740A/D from "Optronics Laboratories, Inc.") with a spectral resolution of 0.2nm that was achieved by using 0.1mm input slit. Instead of the output slit we have used a linear CCD detector with the readout connected to the oscilloscope for the real-time spectrum visualization.

Since both of the lasers are led to the monochromator it is possible to measure the spectrum of both lasers simultaneously while running the experiment in real time. We found this configuration to be extremely helpful for optimization of the position of the pumping beam and detuning of the probing beam to achieve maximum response to a magnetic field.

The monochromator is controlled manually from a special controller. To make the spectrum recording more convenient we have connected it to a computer through a standard analog/digital I/O board from “IoTech, Inc.” model DaqBoard-2000. The wavelength calibration of the monochromator with a linear detector was performed by using a He-Ne laser at 632.8nm.

F) The Faraday modulator and readout electronics

The Faraday modulator consists of a Faraday rotator rod inside a solenoid, which is connected to 2 heat sinks on each side to dissipate the heat produced by the electromagnetic coil. When a current is sent through the solenoid, the generated magnetic field makes the Faraday rotator turn the polarization of a laser. To generate an alternating signal one can set polarizer #1 and polarizer #2 so that no laser light would pass through, also known as maximum extinction. Then an AC current is run through the faraday modulator. The sine wave AC signal was supplied to the modulator coil from a function generator through the power amplifier that could create up to 5A current through an 8 Ohm coil. All measurements were done at about 3˚ modulation amplitude that could be achieved at 1A current through the coil.

The polarization modulation signal was received by a photodiode detector connected to the “Princeton Applied Research” model 126 lock-in amplifier that measured the first harmonic of the modulation signal that is synchronous with the reference signal from the function generator. When the polarization of the light coming from the cesium cell is at maximum extinction for polarizer #2 then only the second harmonic of the signal is present because the transmission through polarizer #2 reaches its peak value in equal proportion during the first and second halves of the modulation period. If the light polarization is slightly rotated due to the cesium vapor dichroism, then the first and second halves of the period will become unequal that

will cause the first harmonic to occur. The value of this harmonic will characterize the magnetic field strength.

IV. Experimental results

After the experimental setup was complete we have made several experiments at different conditions to establish the best operating parameters. Before starting the heating process of the cesium cell, the optical path of the lasers was adjusted for maximum intensity for both the pumping and the probing beams and their wavelengths were set to 894 nm and 894.5 nm respectively. The Faraday modulator amplitude was set to 3˚ and the two polarizers were set to maximum extinction to make the lock-in amplifier most sensitive to polarization changes of the probing beam. By rotating the second polarizer by several degrees from its central position and observing the lock-in amplifier we calibrated the relationship between the voltage sensitivity and the change in the beam polarization and determined it to be (1.1 ± 0.1) mV/deg.

Using a flux-gate magnetometer we have measured the magnetic field inside the shields at the position of the cesium cell. The transverse components that were measured were *Bx=0.1* mG, *Bz=0.14 mG* and a longitudinal component was *By=0.92 mG*. The higher B_y magnetic component was due to a smaller shielding factor for the longitudinal than for the transverse components for a cylindrical shape shield. By using X-Y-Z Hemholtz coils these residual fields was compensated so that all three components were close to zero.

To make sure that no leaks were present in the pressure system the cesium cell was isolated from the pressure regulator and underwent a heating test. The cell was heated from 24 ˚C to 140 ˚C, a process that took about 10 minutes, during which the pressure rose from 10 psi to about 12.6 psi. This rise was caused by the expansion of the helium gas and as well as the rising

vapor pressure of the cesium metal. When the temperature was brought back down to about 30 ˚C the pressure fell back to 10 psi, indicating the absence of helium leaks.

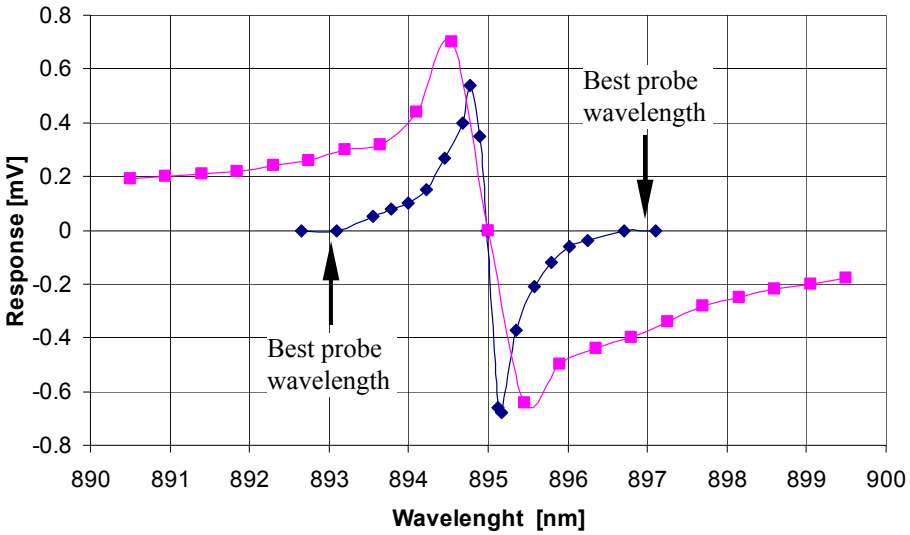

Fig.4. Dependence of the magnetometer response on the wavelength of the probing beam without (blue diamonds) and with (red squares) pumping beam at T = 120 ºC, Fmod = 400 Hz.

When the temperature reached 120 ˚C we were able to observe a well measured response to the change of the longitudinal field created by the *By* coil. To make sure that the observed signal was the expected magnetometer response caused by the interaction of the pumping and the probing beams inside the cell, we simply interrupted the pumping beam with our hand and observed the signal dropping down to zero.

At 120 ˚C we applied a longitudinal field *By* = 2 mG and adjusted the wavelength of the pumping and the probing beam to the maximum response to the applied *By* field. We found that the best pumping wavelength was at 895 nm, this matches the cesium D1 line reported in [16] but slightly differs from other reported D1 line wavelengths ranging from 894 to 894.3nm. [14, 15]. We did not investigate this discrepancy thoroughly because in our case it could be due to the inaccuracy of calibration of the monochromator.

When adjusting the wavelength of the probing beam in the absence of the pumping beam (blue curve in Fig.4) it was found that the output signal strongly depended on the wavelength of

the probing laser. This dependence exists under any magnetic field and thus represents a parasitic signal created by the interaction of the linearly polarized probing beam with the cesium D1 line. The red curve in Fig.4 represents the same probing beam wavelength dependence only now in the presence of the pumping beam. The difference between these two curves represents the useful signal that is dependent on the magnetic field. As follows from the blue curve in Fig.4, the optimum detuning wavelength of the probing beam corresponds to the position where the signal without the pumping beam is zero. At this point the difference between the two curves is close to the maximum value and the useful signal is not affected by the parasitic signal from the probing beam.

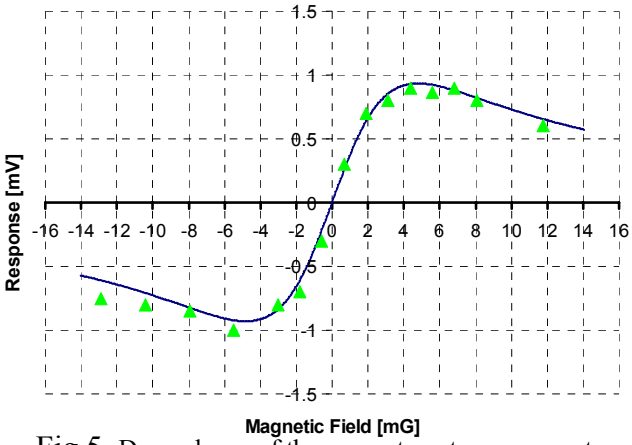

Fig 5. Dependence of the magnetometer response to the magnetic fields.
Triangles – experimental data. Solid line – best fit by the formula (5) at T = 120 ºC.

The dependence of the output signal on the magnetic field measured at 120˚C is shown in Fig.5. It can be seen that the response is almost linear at small magnetic fields and reaches its maximum value at B=5mG. This behavior is a direct consequence of the basic principle of the optical magnetometer. According to equation (2) the polarization precession angle α is changing with a constant angular velocity ω_L that is proportional to the magnetic field B. From (3) it follows that the X-component of spin polarization will reach its maximum value when the initial polarization vector P is rotated by 90˚. If we assume that the precessing spin exists only during that relaxation time, T_r, for which it would make an 180˚ turn, then the average value will be 90˚ which will contribute the most to the rotation of the polarization of the probing beam and consequently to the magnetometer output

voltage. It can easily be seen that if the spin rotates more than 180°, the polarization of the probing beam will rotate in the opposite direction and will decrease the resulting output signal. Following this simplified assumption we can estimate the relaxation time from (1) and (2):

$$T_r = \alpha/\omega_L = \pi/(\gamma \bullet B) \approx 0.18\ s \qquad (4)$$

This estimation however does not take into account the fact that the actual relaxation time is not the same for all cesium atoms but instead obeys a statistical distribution. To accurately calculate its value we should take into account the statistical nature of photon interaction with cesium atoms when it propagates through the vapor cell.

In addition, we found that the observed data at 120 °C can be fitted relatively accurately with the curve shape described by the formula (12) from [7] that represents P_x as a function of magnetic field B in the SERF magnetometer with the similar arrangement. We can rewrite this formula in the following simplified form:

$$Px = K_P \cdot \gamma \cdot B \cdot \frac{R}{(\gamma \cdot B)^2 + (R + T_{SD}^{-1})^2} \qquad (5)$$

where $\gamma = \frac{g_s \mu_B}{\hbar}$ is cesium atom gyromagnetic ratio, R is a pumping rate that is proportional to the number of polarized spins generated in one second, T_{SD} is a spin destruction relaxation time that is supposed to dominate in case of absence of spin exchange relaxation [7]. The scaling coefficient K_P was introduced for fitting the magnetometer voltage response. Assuming $T_{SD} = T_r$ from (4) and using R and K_P as fitting parameters we showed that the measured behavior is in agreement with theory (solid line in Fig.5).

The magnetometer response at different temperatures is shown in Fig.6. It can be seen that at small temperatures the slope, and consequently the magnetometer sensitivity, of the curve at magnetic field equal to zero rises with the temperature because of the increasing vapor

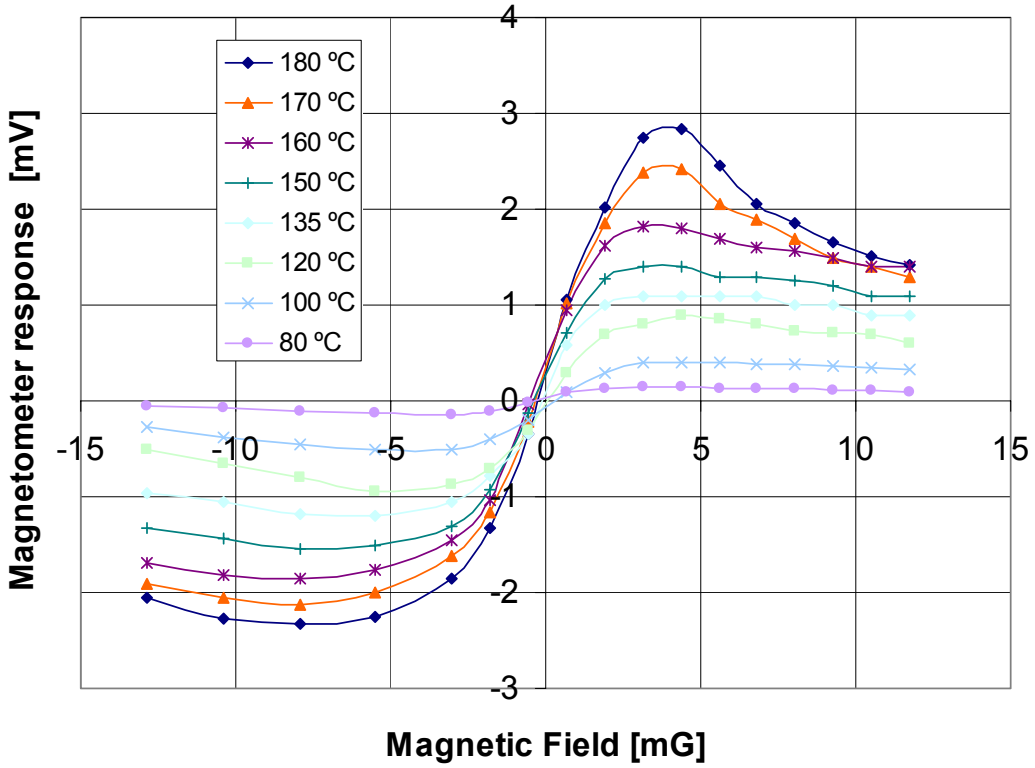

Fig.6. Magnetometer response to a magnetic field *By* at different temperatures.
Fmod = 400 Hz

pressure of the cesium. The slope stops growing at 150 ºC and then even drops slightly when the temperature goes up to 190 ºC. This drop can be explained by the increased probability of collisions between the cesium atoms due to the increase of atomic density, which is equal to the number of molecules per unit of volume, and is described by the R^2 term in the denominator of equation (5) because the pumping rate R is proportional to the atomic density.

The magnetometer dynamic range (the range of magnetic fields where the magnetometer has high sensitivity) as seen from Fig.5 is always rising with temperature in spite of the fact that the shape started to be pretty asymmetrical after 135 ºC so the signal saturates slowly at negative magnetic fields.

To characterize the possibility of the magnetometer to work in non shielded environment we recorded the dependence of the magnetometer response at *By* =1.5 mG on the transversal magnetic field Bz (see Fig.7).

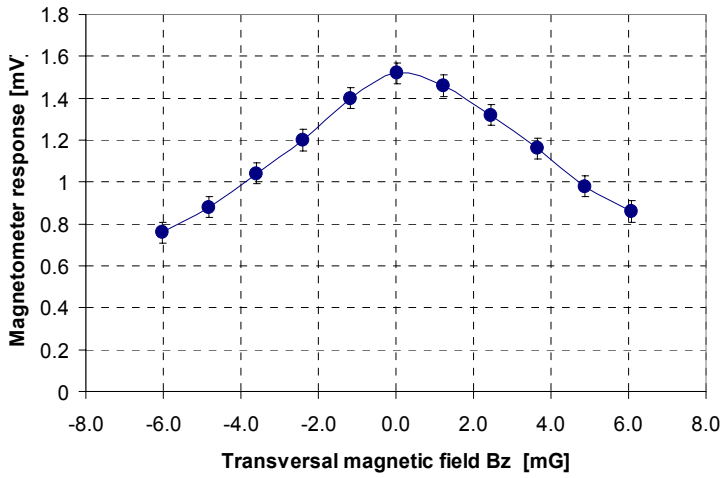

Fig.7. Magnetometer response dependence on transversal magnetic field Bz at By = 1.5 mG.
T = 180 ºC, Fmod = 400 Hz

The graph shows that the ambient magnetic field can easily degrade the sensitivity of the magnetometer and therefore the removal of shields can completely suppress the magnetometer operation in the magnetic field of the earth which is about 500 mG. However if the ambient field is compensated to less then 4 mG with X-Y-Z Hemholtz coils then the sensitivity will drop by a factor of two only and will be still enough for many practical applications.

V. Conclusion

We have built an experimental setup with an optical magnetometer that utilizes important advantages of Spin-Exchange Relaxation Free (SERF) femtotesla-scale magnetometer [7], such as a very small (< 1cm^3) measurement volume and completely optical pumping/probing beam readout arrangement. This magnetometer configuration is expected to work best for future multi-channel imaging applications where several magnetometers will be arranged in the form of a two-dimensional array to perform the real-time mapping of magnetic field distribution.

The magneto sensitive part of the setup including the vapor cell, optical components and the heating system is made of completely non-magnetic materials such as wood, glass, rubber and plastic. The real time pressurization system enables filling the cell with a buffer gas (He^4) and regulating its pressure from 0 to 3 atm without interrupting the measurements.

Two non-expensive tunable laser sources with 0.15 nm line width and 10 nm tuning range were developed and built out of commercially available parts. They served as excellent pumping and probing beam sources in the magnetometer setup, which eliminated the need for expensive tunable laser systems that cost more than $10,000.

The use of a cesium that has higher saturated vapor pressure [17], enabled operation of a magnetometer at much lower temperatures then the similar setup with potassium [7]. We found that the magnetometer began operating at 80˚C and reached a maximum sensitivity at 150˚C while potassium magnetometer required 190˚C for proper operation.

The sensitivity of the magnetometer to the magnetic field found from the slope at B = 0 mG is about 0.9 mV/mG. The noise measured at the output of the lock-in amplifier at 400 Hz Faraday modulation frequency was $4.1 \bullet 10^{-3}$ mV/Hz$^{1/2}$ that gives the estimation of field sensitivity of $4.5 \bullet 10^{-10}$ T/Hz$^{1/2}$ in the active volume of 3 mm^3 that is currently formed by cross sections of 3x0.5 mm^2 probing beam and 3x2 mm^2 pumping beam. Since the sensitivity can be improved proportionally to the square root of the active volume [7], increasing the volume to 1 cubic inch will improve the sensitivity by a factor of 74. Another improvement by a factor of 10 can be reached by using a more powerful laser that produces lower noise that all together will give a sensitivity of 0.6 pT/Hz$^{1/2}$. This sensitivity seems to be enough for building a multi-channel magnetometer for cardio-magnetic imaging that deals with about 2 – 10 pT magnetic fields produced by the human heart.

References

[1] D. Drung, S. Bechstein, K.P. Franke, M. Scheiner and T. Schurig. "Improved direct-coupled dc SQUID read-out electronics with automatic bias voltage tuning", IEEE T. Appl. Supercon **11**:880-883 (2001).

[2] N. Oukhanski, R. Stolz, V. Zakosarenko and H.G. Meyer. "Low-drift broadband directly coupled dc SQUID read-out electronics," Physica C **368**:166-170 (2002).

[3] D. Koelle, R. Kleiner, F. Ludwig, E. Dantsker, and J. Clarke. "High-transition-temperature superconducting quantum interference devices", Reviews of Modern Physics **71**: 631-686 (1999).

[4] J. Dupont-Roc, S. Haroche and C. Cohen-Tannoudji, "Detection of very weak magnetic fields (10-9gauss) by 87Rb zero-field level crossing resonances," Phys. Lett. A **28**: 638-639 (1969).

[5] E. B. Aleksandrov, M. V. Balabas, A. K. Vershovskii, A. E. Ivanov, N. N. Yakobson , V. L. Velichanskii, N. V. Senkov, "Laser pumping in the scheme of an Mx-magnetometer," Optics and Spectr **78**: 292-298 (1995).

[6] D. Budker, D. F. Kimball, S. M. Rochester, V. V. Yashchuk, M. Zolotorev, "Sensitive magnetometry based on nonlinear magneto-optical rotation," Phys. Rev. A **62**: 043403 (2000).

[7]. T.W. Kornack and M. V. Romalis, "High-Sensitivity Atomic magnetometer Unaffected by Spin-Exchange Relaxation, " Physical review Letters, **89**, 130801 (2002).

[8] G. Bison, R. Wynands, A. Weis, "A laser-pumped magnetometer for the mapping of human cardio-magnetic fields," Appl. Phys. B **76**: 325-328 (2003).

[9] G. Bison, R. Wynands, A. Weis, "Dynamical mapping of the human cardio magnetic field with a room-temperature, laser-optical sensor," Optics Express **11**, 904 (2003).

[10] V.V. Yashchuk, D. Budker, and M. Zolotorev, "Applications of Nonlinear Magneto-Optic Effects with Ultra-Narrow Widths," Trapped Charged Particles and Fundamental Physics, D.H.E. Dubin and D. Schneider, eds. AIP conference proceedings 457, pp. 177-181.

[11] E.B. Alexandrov, M.V. Balabas, and V.A. Bonch-Bruevich, Sov. Tech. Phys. Lett. **13,** 312 (1987).

[12] S. B. Bayram, T.E. Chupp, "Operation of a single mode external cavity laser diode near 780 nm," Review of Scientific instruments **73**, 4169 (2002).

[13] C.J. Hawthorn, K. P. Weber, and R. E. Scholten, "Littrow configuration tunable external cavity diode laser with fixed direction output beam," Review of Scientific Instruments **72**, 4477 (2001).

[14] R. Beuc, H. Skenderovic, T. Ban, D. Veza, G. Pichler, and W. Meyer, "Cesium satellite band at 875.2 nm stemming from the Cs_2 O^+_g ($6p^2\,P_{1/2} + 6s^2\,S_{1/2}$) state," European Physical Journal D **15,** 209-214 (2001).

[15] A. Andalkar, S.K. Lamoreaix, R.B. Warrington, " External Cavity Diode Laser System for Cesium D1 (894 nm)," Department of Physics at University of Washington, Seattle, WA (1999), submitted for publication.

[16] Th. Udem, J. Reichert, R. Holzwarth, and T.W. Hansch, "Absolute optical Frequency Measurement of the Cesium D_1 Line with a Mode-Locked Laser," Physical Review Letters **82,** 3568 (1999).

[17] A. N. Nesmeyanov, *Vapor pressure of the Chemical Elements*, R. Gray (Ed.), Elsevier, Amsterdam-London-New York, 1963.